Available online at www.sciencedirect.com
ScienceDirect
International Journal of Solids and Structures 43 (2006) 6014–6025
INTERNATIONAL JOURNAL OF SOLIDS and STRUCTURES
www.elsevier.com/locate/ijsolstr

Modelling of bonded multilayered disks subjected to biaxial flexure tests

C.H. Hsueh *, C.R. Luttrell, P.F. Becher

Metals and Ceramics Division, Oak Ridge National Laboratory, P.O. Box 2008, Oak Ridge, TN 37831, USA

Received 19 May 2005
Available online 21 September 2005

Abstract

Biaxial flexure tests have been used extensively for the strength measurements of monolithic brittle materials. However, despite the increasing applications of multilayered structures, characterization of their strengths using biaxial flexure tests is unavailable. This is because the analytical description of the relation between the strength and the fracture load for multilayers subjected to biaxial flexure tests is nonexistent. To characterize the biaxial strength of multilayers, an analytical model is developed in the present study to derive the general closed-form solutions for the elastic stress distributions in thin multilayered disks subjected to biaxial flexure tests. To verify the analytical solutions, finite element analyses are performed on trilayered disks subjected to ring-on-ring tests. Good agreement is obtained between analytical and numerical results. The present closed-form solutions hence provide a basis for evaluating the biaxial strength of multilayered systems. Depending upon the strength of the individual layers and the stress distribution through the thickness of the multilayer during testing, cracking can initiate from any layer under tension.

Keywords: Modelling; Biaxial flexure; Multilayers; Disk; Finite element; Stress

1. Introduction

Multilayered structures have extensive applications as microelectronic, optical, structural, and biological components. To maintain the functionality and reliability of multilayered systems, it is essential to understand the geometrical and material factors that influence their strength. Uniaxial strength tests, such as three- or four-point bending of bars, have been used extensively in the past to determine the strength of brittle materials (Brett et al., 1990; Skorvánek and Gerling, 1992; Arai et al., 1994). However, the measured

* Corresponding author. Tel.: +1 865 576 6586; fax: +1 865 574 6098.
E-mail address: hsuehc@ornl.gov (C.H. Hsueh).

0020-7683/$ - see front matter
doi:10.1016/j.ijsolstr.2005.07.020

strength depends on both the surface and the edge conditions, and it is very difficult to eliminate undesirable edge failures (Ritter et al., 1980). On the other hand, biaxial flexure tests involve supporting a thin plate on three or more points near its periphery and equidistant from its center and loading a central portion. The area of maximum tensile stress thus falls at the center of the plate surface and the measured strength is independent of the condition of the plate edges. Also, real material components are generally subjected to multiaxial loading during service applications, and the biaxial strength data are more useful than the uniaxial strength data for the material design. As a result, biaxial flexure tests, such as ball-on-ring (or ball-on-three-ball), ring-on-ring, and piston-on-three-ball tests, are becoming increasingly popular as a means of measuring the strength of brittle materials (Shetty et al., 1980; Lucas, 1990; Meyers et al., 1993; Hehn et al., 1994; Zeng et al., 1998; Shi et al., 1998; Simpatico et al., 1999; Li et al., 2001).

Stress analyses for biaxial flexure tests are very complex even for monolithic elastic materials. A method of handling a thin monolayered disk supported at several points along its boundary and subjected to normal loadings symmetrically distributed over a concentric circular area was first developed by Nadai (1922). The relation between the transverse displacement of the disk and the load intensity was described by a biharmonic equation, and its general solution could be obtained using Muskhelishvili's complex variable method (Muskhelishvili, 1949). Solving the biharmonic equation with the essential equilibrium conditions and boundary conditions is a difficult task, and Bassali (1957) was able to obtain a complex series solution. However, because of the complex formulation, application of Bassali's solution is quite difficult. As a result, Bassali's solution was subsequently simplified by Vitman and Pukh (1963) and Kirstein and Woolley (1967) to expressions that could be easily adapted to the design and analysis of thin disks. However, the existing expression is applicable only when the disk is monolithic. When the disk has a multilayered structure, the continuity conditions at the interfaces between layers are required in analyses, and the solutions have not been derived up to date. In the absence of closed-form solutions for multilayered disks subjected to biaxial flexure tests, the finite element analysis (FEA) has been performed to analyze trilayers subjected to ring-on-ring tests (Selcuk et al., 2001). Although the FEA provides a powerful means for analyzing stress fields in complex multilayered systems, it suffers from the drawback that it is a case-by-case study and computation needs to be performed for each change in geometrical parameters and material properties. Hence, in order to measure the strength of multilayers using biaxial flexure tests, it is essential to develop an analytical model to analyze this problem.

The purpose of the present study is to derive a closed-form solution to relate the strength to the fracture load for thin multilayered disks subjected to biaxial flexure tests. First, an analytical model is developed to derive the stress distributions in multilayered disks subjected to biaxial flexure tests. This is achieved by satisfying the continuity condition at the interfaces between layers as well as the force and moment equilibrium conditions for the multilayered system and utilizing the existing closed-form solutions for monolayered discs. Then, an application of the solutions to determine the film modulus for a film/substrate bilayered system using biaxial flexure tests is discussed. Second, the FEA is performed on multilayered disks subjected to ring-on-ring tests. Finally, the comparison between the analytical and the finite element results is made to validate the present closed-form solutions for multilayered systems.

2. Analyses

A thin multilayered disk is considered. A diametrical section through the axis of symmetry of the multilayered disk is shown schematically in Fig. 1. The disk consists of n layers with individual thickness, t_i, where the subscript, i, denotes the layer number with layer 1 being at the bottom of the disk. The cylindrical coordinates, r, θ, and z, are used. The bottom surface of layer 1 is located at $z = 0$, the interface between layers i and $i + 1$ is located at h_i, and the top surface of layer n is located at $z = h_n$. With these definitions, h_n is the thickness of the disk, and the relation between h_i and t_i is described by

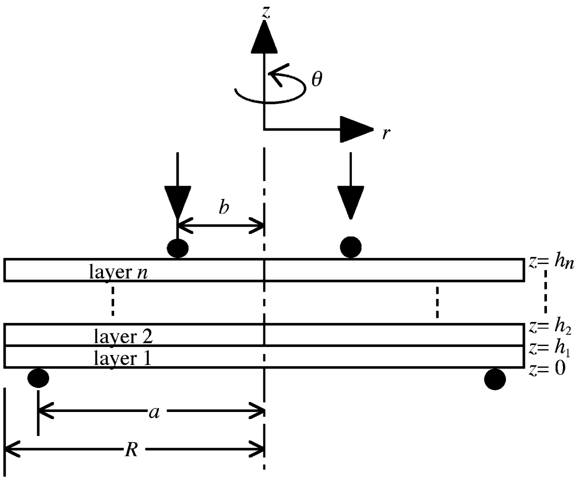

Fig. 1. A schematic showing the diametrical section through the axis of symmetry of a multilayered disk subjected to ring-on-ring tests.

$$h_i = \sum_{j=1}^{i} t_j \quad (i = 1\text{–}n). \tag{1}$$

The disk is subjected to biaxial flexure tests, and the interfaces between layers are assumed to remain bonded during tests. The stress distributions in the multilayered disk can be determined from the force and moment equilibrium conditions coupled with the existing solutions for monolayered disks, and the analytical procedures are described in the following.

For small deflection (e.g., less than one-quarter of the disk thickness), the strains are proportional to the distance from the neutral surface and inversely proportional to the radius of curvature (Timoshenko and Woinowsky-Krieger, 1959). For a monolayered disk, the neutral surface coincides with the middle plane of the disk. However, for a multilayered disk, the neutral surface deviates from the middle plane because of the nonuniform elastic properties through the disk thickness. The radial and the tangential strains, ε_r and ε_θ, in the system are (Timoshenko and Woinowsky-Krieger, 1959):

$$\varepsilon_r = \frac{z - z_{nr}}{r_r} \quad (0 \leqslant z \leqslant h_n), \tag{2a}$$

$$\varepsilon_\theta = \frac{z - z_{n\theta}}{r_\theta} \quad (0 \leqslant z \leqslant h_n), \tag{2b}$$

where $z = z_{nr}$ and $z = z_{n\theta}$ dictate the positions of neutral surfaces for bending in the radial and the tangential directions, respectively, and r_r and r_θ are the corresponding radii of curvature. It should be noted that by using Eq. (2) to describe the strain distribution in the system, the strain-continuity condition at the interfaces is automatically satisfied. For a thin disk, the stress normal to the disk is negligible, and the radial and the tangential stresses, σ_r and σ_θ, are related to strains by

$$\sigma_{ri} = E_i^*(\varepsilon_r + \nu_i\varepsilon_\theta) \quad (i = 1\text{–}n), \tag{3a}$$

$$\sigma_{\theta i} = E_i^*(\varepsilon_\theta + \nu_i\varepsilon_r) \quad (i = 1\text{–}n), \tag{3b}$$

where $E_i^* = E_i/(1 - \nu_i^2)$ is the plane-strain modulus, E and ν are Young's modulus and Poisson's ratio, respectively, and the subscript, i, denotes the layer number.

There is no in-plane applied force, and the force equilibrium condition requires

$$\sum_{i=1}^{n}\int_{h_{i-1}}^{h_i}\sigma_{ri}\,\mathrm{d}z = 0, \tag{4a}$$

$$\sum_{i=1}^{n}\int_{h_{i-1}}^{h_i}\sigma_{\theta i}\,\mathrm{d}z = 0. \tag{4b}$$

When $i = 1$, h_{i-1} (i.e., h_0) in Eqs. (4a) and (4b) is defined as zero. The positions of the two neutral planes can be obtained by substituting Eqs. (2) and (3) into Eqs. (4a) and (4b). It is found that solutions of z_{nr} and $z_{n\theta}$ are complex and they are functions of the two radii of curvature. However, solutions are greatly simplified if the difference between v_i ($i = 1$–n) is ignored in the parentheses in Eqs. (3a) and (3b). Using this simplification [i.e., letting $v_i = v$ in the parentheses in Eqs. (3a) and (3b)], z_{nr} and $z_{n\theta}$ become independent of both the two radii of curvature and v, and their solutions are

$$z_{nr} = z_{n\theta} = z_n = \frac{\sum_{i=1}^{n}E_i^* t_i\left(h_{i-1} + \frac{t_i}{2}\right)}{\sum_{i=1}^{n}E_i^* t_i}. \tag{5}$$

In this case, the two neutral surfaces become one and it is redefined as z_n. It should be noted that the simplification of Poisson's ratio v_i in the plane-strain modulus, $E_i/(1 - v_i^2)$, in Eqs. (3a) and (3b) is not required in order to obtain Eq. (5). Hence, in the present analysis, E_i^* should be regarded as one term without the simplification in v_i.

The moment equilibrium condition requires

$$\sum_{i=1}^{n}\int_{h_{i-1}}^{h_i}\sigma_{ri} z\,\mathrm{d}z = M_r, \tag{6a}$$

$$\sum_{i=1}^{n}\int_{h_{i-1}}^{h_i}\sigma_{\theta i} z\,\mathrm{d}z = M_\theta, \tag{6b}$$

where M_r and M_θ are bending moments per unit length. Solutions of Eqs. (6a) and (6b) yield

$$M_r = D\left(\frac{1}{r_r} + v\frac{1}{r_\theta}\right), \tag{7a}$$

$$M_\theta = D\left(\frac{1}{r_\theta} + v\frac{1}{r_r}\right), \tag{7b}$$

where D has the physical meaning of the flexural rigidity of the multilayer and is

$$D = \sum_{i=1}^{n}E_i^* t_i\left[h_{i-1}^2 + h_{i-1}t_i + \frac{t_i^2}{3} - \left(h_{i-1} + \frac{t_i}{2}\right)z_n\right], \tag{8}$$

where z_n is given by Eq. (5). Combining Eqs. (3a) and (3b) with Eqs. (7a) and (7b), the stresses can be related to bending moments by

$$\sigma_{ri} = \frac{E_i^*(z - z_n)M_r}{D} \quad (i = 1\text{–}n), \tag{9a}$$

$$\sigma_{\theta i} = \frac{E_i^*(z - z_n)M_\theta}{D} \quad (i = 1\text{–}n). \tag{9b}$$

For a monolayered disk with uniform material properties, $E_i = E$ and $v_i = v$, Eqs. (5) and (8) become

$$z_n = \frac{h_n}{2}, \tag{10}$$

$$D = \frac{E^* h_n^3}{12}, \tag{11}$$

where $E^* = E/(1 - \nu^2)$. Eqs. (10) and (11) recover the neutral surface and the flexural rigidity of a monolayered disk (Timoshenko and Woinowsky-Krieger, 1959). Also, in this monolayer-case, the stresses are related to bending moments by

$$\sigma_r = \frac{12(z - z_n)M_r}{h_n^3}, \tag{12a}$$

$$\sigma_\theta = \frac{12(z - z_n)M_\theta}{h_n^3}, \tag{12b}$$

where z_n is given by Eq. (10). Comparing Eqs. (9a) and (9b) with Eqs. (12a) and (12b), the stress distributions in a multilayered disk can be obtained from those of a monolayer disk by multiplying the factor, F_i, for stresses in layer i; i.e.,

$$\sigma_{ri} = F_i \sigma_r \quad (i = 1\text{–}n), \tag{13a}$$

$$\sigma_{\theta i} = F_i \sigma_\theta \quad (i = 1\text{–}n), \tag{13b}$$

where

$$F_i = \frac{E_i^* h_n^3}{\sum_{i=1}^n 2E_i^* t_i [6h_{i-1}^2 + 6h_{i-1}t_i + 2t_i^2 - 3(2h_{i-1} + t_i)z_n]} \quad (i = 1\text{–}n). \tag{14}$$

Also, it should be noted that while the position of the neutral surface is given by Eq. (10) for the monolayer, it is given by Eq. (5) for the multilayer.

2.1. Bilayered disks

For the special case of bilayered disks; i.e., $n = 2$, Eqs. (5) and (8) become

$$z_n = \frac{E_1^* t_1^2 + E_2^* t_2 (2t_1 + t_2)}{2\left(E_1^* t_1^2 + E_2^* t_2\right)}, \tag{15}$$

$$D = E_1^* t_1^2 \left(\frac{t_1}{3} - \frac{z_n}{2}\right) + E_2^* t_2 \left[t_1^2 + t_1 t_2 + \frac{t_2^2}{3} - \left(t_1 + \frac{t_2}{2}\right) z_n\right]. \tag{16}$$

When $t_1 \gg t_2$ (e.g., for film/substrate systems), Eqs. (15) and (16) can be simplified, such that

$$z_n = \frac{t_1}{2} + \frac{E_2^* t_2}{2E_1^*}, \tag{17}$$

$$D = \frac{E_1^* t_1^3}{12} + \frac{E_2^* t_1^2 t_2}{4}. \tag{18}$$

Hence, by measuring the difference in the flexure rigidity between the substrate and the film/substrate systems, Eq. (18) can be used to determine modulus of the film, E_2^*.

2.2. Ring-on-ring tests on multilayered disks

For ring-on-ring tests, the specimen is supported by an outer ring and loaded with a smaller coaxial inner ring. The approximate analytical solutions for stress distributions in monolayer disks have been obtained, and the central region bounded by the inner ring is subjected to biaxial stress that is uniform with respect to r and θ directions. These stresses on the tensile surface are (Kirstein and Woolley, 1967; Shetty et al., 1980):

$$\sigma_r = \sigma_\theta = \frac{3P}{4\pi h_n^2}\left[2(1+v)\ln\left(\frac{a}{b}\right) + \frac{(1-v)(a^2-b^2)}{R^2}\right] \quad (\text{for } r \leqslant b \text{ and } z=0), \tag{19a}$$

$$\sigma_r = \frac{3P}{4\pi h_n^2}\left[2(1+v)\ln\left(\frac{a}{r}\right) + \frac{(1-v)b^2(a^2-r^2)}{r^2R^2}\right] \quad (\text{for } r > b \text{ and } z=0), \tag{19b}$$

$$\sigma_\theta = \frac{3P}{4\pi h_n^2}\left[2(1+v)\ln\left(\frac{a}{r}\right) - \frac{(1-v)b^2(a^2+r^2)}{r^2R^2} + 2(1-v)\frac{a^2}{R^2}\right] \quad (\text{for } r > b \text{ and } z=0), \tag{19c}$$

where P is the load, and a, b, and R are the radii of outer ring, inner ring, and the disk, respectively. Considering the linear stress distribution through the disk thickness, the variations of stresses through the thickness are described by

$$\sigma_r = \sigma_\theta = \frac{-3P\left(z-\frac{h_n}{2}\right)}{2\pi h_n^3}\left[2(1+v)\ln\left(\frac{a}{b}\right) + \frac{(1-v)(a^2-b^2)}{R^2}\right] \quad (\text{for } r \leqslant b \text{ and } 0 \leqslant z \leqslant h_n), \tag{20a}$$

$$\sigma_r = \frac{-3P\left(z-\frac{h_n}{2}\right)}{2\pi h_n^3}\left[2(1+v)\ln\left(\frac{a}{r}\right) + \frac{(1-v)b^2(a^2-r^2)}{r^2R^2}\right] \quad (\text{for } r > b \text{ and } 0 \leqslant z \leqslant h_n), \tag{20b}$$

$$\sigma_\theta = \frac{-3P\left(z-\frac{h_n}{2}\right)}{2\pi h_n^3}\left[2(1+v)\ln\left(\frac{a}{r}\right) - \frac{(1-v)b^2(a^2+r^2)}{r^2R^2} + 2(1-v)\frac{a^2}{R^2}\right] \quad (\text{for } r > b \text{ and } 0 \leqslant z \leqslant h_n). \tag{20c}$$

When Eq. (20) is extended to the multilayer-case, v should be regarded as the average Poisson's ratio of the disk, such that

$$v = \frac{1}{h_n}\sum_{i=1}^{n} v_i t_i. \tag{21}$$

Hence, the stress distributions in multilayered disks subjected to ring-on-ring tests are

$$\sigma_{ri} = \sigma_{\theta i} = \frac{-3F_iP(z-z_n)}{2\pi h_n^3}\left[2(1+v)\ln\left(\frac{a}{b}\right) + \frac{(1-v)(a^2-b^2)}{R^2}\right] \quad (\text{for } r \leqslant b \text{ and } i = 1\text{–}n), \tag{22a}$$

$$\sigma_{ri} = \frac{-3F_iP(z-z_n)}{2\pi h_n^3}\left[2(1+v)\ln\left(\frac{a}{r}\right) + \frac{(1-v)b^2(a^2-r^2)}{r^2R^2}\right] \quad (\text{for } r > b \text{ and } i = 1\text{–}n), \tag{22b}$$

$$\sigma_{\theta i} = \frac{-3F_iP(z-z_n)}{2\pi h_n^3}\left[2(1+v)\ln\left(\frac{a}{r}\right) - \frac{(1-v)b^2(a^2+r^2)}{r^2R^2} + 2(1-v)\frac{a^2}{R^2}\right] \quad (\text{for } r > b \text{ and } i = 1\text{–}n), \tag{22c}$$

where z_n and F_i are given by Eqs. (5) and (14), respectively. Depending upon the comparison between the strength of the individual layers and the stress distribution through the thickness of the multilayer during testing, cracking can initiate from any layer under tension, and Eq. (22) provides a basis for evaluating the biaxial strength of multilayered systems. It should be noted that Eqs. (13) and (14) are valid for any biaxial flexure test in converting monolayer-solutions to multilayer-solutions. While solutions are listed specifically for ring-on-ring tests here, the solutions for other biaxial flexure tests can be formulated accordingly.

3. Finite element analysis

In order to validate the analytical solution, the FEA is used to simulate results for ring-on-ring tests on both monolayered and trilayered disks. While the simulated results for monolayered disks are compared with existing solutions, Eqs. (19) and (20), to examine the accuracy, the simulated results for trilayered disks are compared with the present closed-form solutions, Eqs. (22a), (22b) and (22c), to validate the present analytical solutions. The algorithm models frictionless contact between rings and the specimen, and the interfaces between layers are assumed to remain bonded at all stages of computation. The monolayered and trilayered disks are modelled using 8-node curved shell elements in the finite element code ABAQUS version 6.4-1. The outer ring constraint is modelled by fixing the nodes of the elements at the outer ring location in the vertical direction. The nodes are free to move in the other directions. At the location of the loading ring, a pressure is applied over a small area to apply the desired load.

4. Results

Specific results are calculated using materials properties pertinent to yttria stabilized zirconia (YSZ) monolayer and solid oxide fuel cells (SOFC) trilayer subjected to ring-on-ring tests in order to elucidate the essential trends. The YSZ monolayer has a thickness of 150 μm. The SOFC trilayer consists of $La_{0.75}Sr_{0.2}MnO_3$ (LSM) cathode layer of 25 μm thickness, YSZ electrolyte layer of 150 μm thickness, and NiO-YSZ anode layer of 25 μm thickness. The specimens have a radius, R, of 25 mm, and the materials properties are listed in Table 1 (Selcuk et al., 2001). It should be noted that both the cathode and the anode layers are porous, their stress–strain relations can be nonlinear. For example, pores can form cracks and propagate during loading which, in turn, can result in decreasing modulus with increasing load. Also, depending upon the shape and the orientation of pores, the elastic properties of porous materials can be anisotropic. Both nonlinearity and anisotropy in elastic properties of porous materials are not considered in the present study. The supporting and the loading rings have radii of $a = 19$ mm and $b = 4.75$ mm, respectively, and $P = 10$ N is loaded on the specimen through the loading ring. The results for other loads can be obtained by scaling with the load because of the linear elasticity used in analyses. However, it should be noted that because the deflection is generally limited to less than one-quarter of the disk thickness in order to satisfy the condition of small deflection during tests, the corresponding load is also subjected to this constraint. The FEA mesh used for modelling the monolayered and trilayered disks is shown in Fig. 2. The disks are modelled using 1/4 symmetry. The mesh consists of 279 elements and 913 nodes, and it is biased towards the center of the disk such that the smallest elements are located in the central area.

For the YSZ monolayered disk, both the radial and the tangential stresses, σ_r and σ_θ, on the tensile surface of the specimen; i.e., at $z = 0$ in Fig. 1, as functions of the radial distance from the center of the disk, r, are shown in Fig. 3(a). Eq. (19) shows that the stress has a maximum in the region of $r \leqslant b$ and decays with the distance from the center, and the radial stress on the tensile surface becomes compressive in the overhang region, $r \geqslant a$. While good agreement between Eq. (19a) and FEA is shown in the region of $r \leqslant b$, discrepancy is observed between Eqs. (19b) and (19c) and FEA in the region of $r > b$. This is mainly due to the fact that Eq. (19) is a simplified approximate solution. Specifically, Eq. (19b) shows that the radial stress, σ_r, is zero at $r = a$ and has a finite value at $r = R$ which violates the free-surface condition at the disk edge. Also, the FEA results show a small peak in σ_r on the tensile surface opposite and just inside the loading ring position (which can hardly be seen in Fig. 3(a)). This small peak results from the contact stress.

Table 1
Elastic properties of LSM/YSZ/NiO-YSZ trilayer

Materials	E (GPa)	v
LSM	35	0.25
YSZ	215	0.32
NiO-YSZ	55	0.17

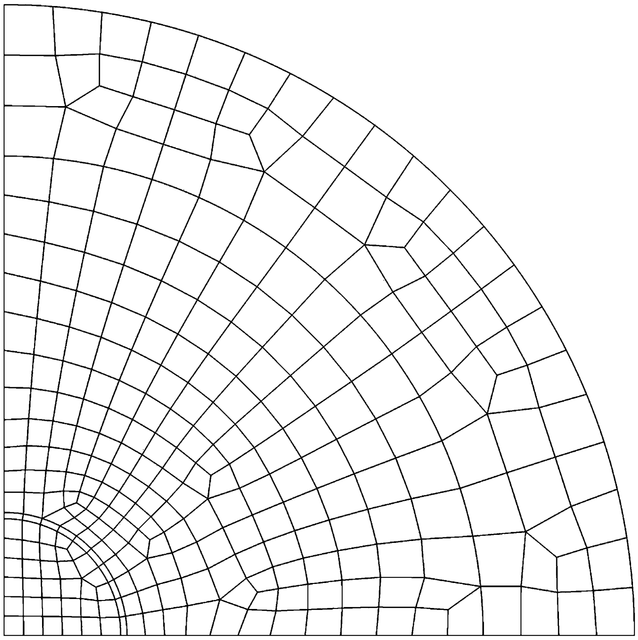

Fig. 2. The finite element mesh for a disk subjected to ring-on-ring tests.

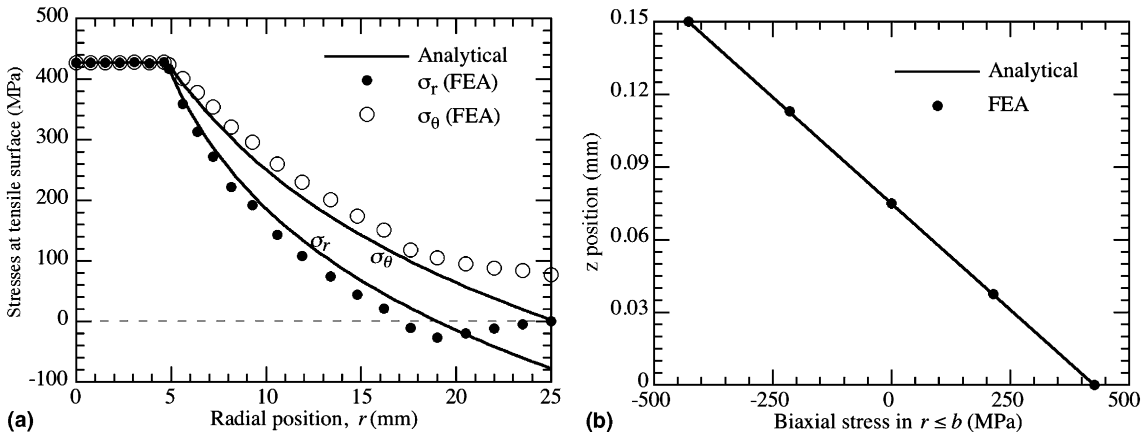

Fig. 3. (a) The radial and tangential stresses, σ_r and σ_θ, at the tensile surface, and (b) biaxial stresses, σ_r ($=\sigma_\theta$), in the region of $r \leqslant b$ through the thickness of a YSZ monolayered disk subjected to ring-on-ring tests showing the comparison between analytical and FEA results.

Because analytical modelling considers only the flexural stress due to biaxial flexure loading not the contact stress, it cannot predict this peak stress. However, using FEA, the above discrepancy and peak stress are both found to be diminished as the overhang region becomes smaller (i.e., as $R \to a$). Also, because only Eq. (19a) is required to relate the biaxial strength to the fracture load for monolayered disks, the inaccuracy of Eqs. (19b) and (19c) is not of concern. The biaxial stress, $\sigma_r = \sigma_\theta$, in the region of $r \leqslant b$ and through the specimen thickness is shown in Fig. 3(b). The stress is linear, and excellent agreement is obtained between Eq. (20a) and FEA results.

For the LSM/YSZ/NiO-YSZ trilayered disk, modelling is performed such that LSM is the tensile layer; i.e., layer 1 in Fig. 1. Both the radial and the tangential stresses, σ_r and σ_θ, on the tensile surface of the specimen as functions of r are shown in Fig. 4(a). Like Eq. (19), Eq. (22) shows that the stress has a maximum in the region of $r \leqslant b$ and decays with the distance from the center, and the radial stress on the tensile surface becomes compressive in the overhang region, $r \leqslant a$. In the region of $r \leqslant b$, the stress predicted from Eq. (22a) is greater than that from FEA by ~3.5%, and this difference will be discussed later. In the region of $r > b$, discrepancy is observed between Eqs. (22b) and (22c) and FEA. While the present closed-form solutions for multilayers are derived by utilizing the existing solutions for monolayers, they also inherit the inaccuracy in the region of $r > b$. The biaxial stress, $\sigma_r = \sigma_\theta$, in the region of $r \leqslant b$ and through the specimen thickness is shown in Fig. 4(b). The stress is linear through the thicknesses in each individual layer; however, because of different elastic properties among the three layers, the (in-plane) stress is discontinuous at the interfaces and the stress gradients are different. Good agreement between the analytical and the FEA results validates the present closed-form solutions for multilayers, Eq. (22). In this trilayer-case, the greatest tension does not occur at the tensile surface of the specimen; instead, it exists at the lower surface of the middle (i.e., YSZ) layer. This is because the YSZ layer is much stiffer than the LSM layer. Depending upon the comparison between the strength and the maximum tension in each layer, cracking can initiate in the inner layer instead of at the tensile surface of the specimen. Also, it can be seen in Fig. 4(b) that the compared to the FEA results, the analytical solutions slightly under-predict the magnitude of stresses in the YSZ layer (by 2%) and over-predict the magnitude of stresses in both the LSM (by 3.5% see also Fig. 4(a)) and the NiO-YSZ (by 10%) layers. This is because the difference in Poisson's ratio between layers is ignored in the parentheses in Eqs. (3a) and (3b) when the position of the neutral surface is determined analytically, and the average Poisson's ratio of the trilayer, v [see Eq. (21)], is used. While v of the trilayer layer is 0.29, it is greater than the actual Poisson's ratios of both LSM (0.25) and NiO-YSZ (0.17) but is lower than the Poisson's ratio of YSZ (0.32). As a result, when v_i in the parentheses in Eqs. (3a) and (3b) is replaced by v, stresses in both LSM and NiO-YSZ are over-predicted while stresses in YSZ are under-predicted. Also, because the NiO-YSZ layer has the biggest difference between v_i and v among the three layers, it incurs the biggest discrepancy between the analytical and FEA results. To verify this,

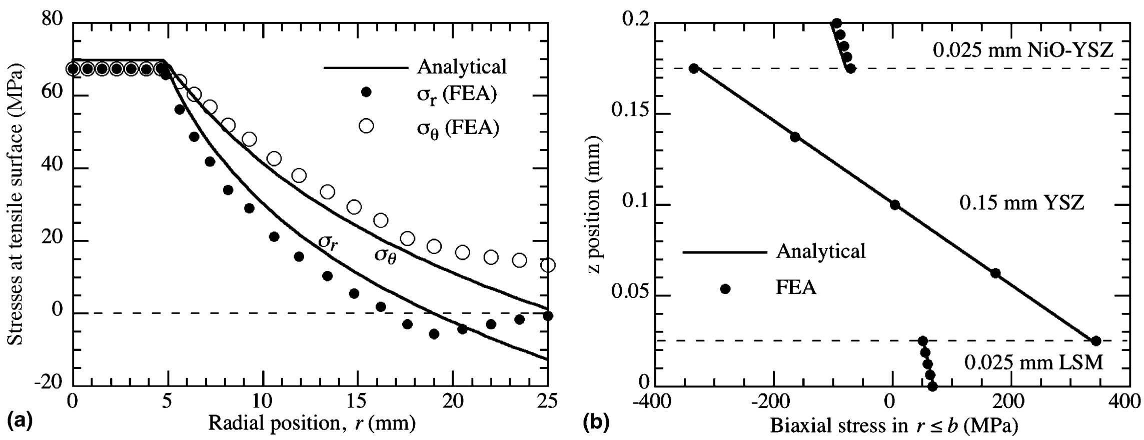

Fig. 4. (a) The radial and tangential stresses, σ_r and σ_θ, at the tensile surface, and (b) biaxial stresses, σ_r $(=\sigma_\theta)$, in the region of $r \leqslant b$ through the thickness of an LSM/YSZ/NiO-YSZ trilayered disk subjected to ring-on-ring tests showing the comparison between analytical and FEA results.

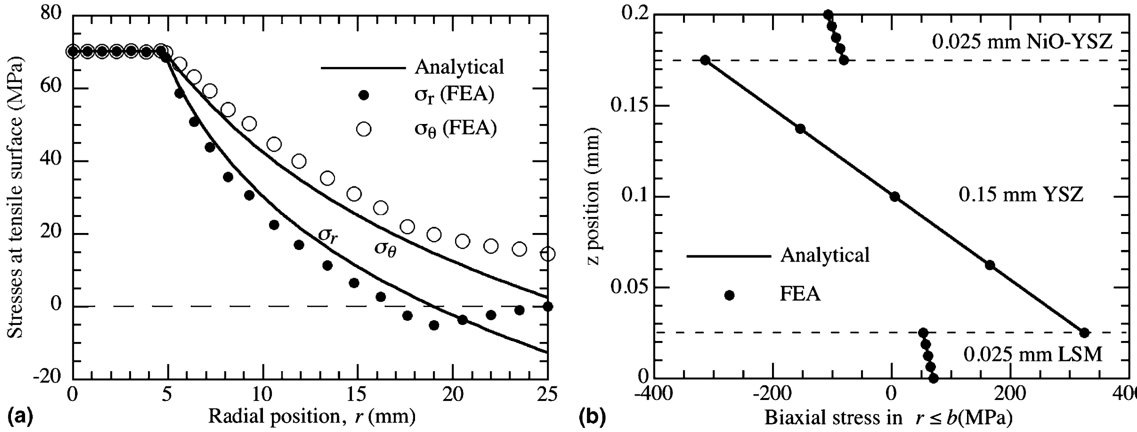

Fig. 5. (a) The radial and tangential stresses, σ_r and σ_θ, at the tensile surface, and (b) biaxial stresses, σ_r $(=\sigma_\theta)$, in the region of $r \leqslant b$ through the thickness of an LSM/YSZ/NiO-YSZ trilayered disk subjected to ring-on-ring tests showing the comparison between analytical and FEA results. Poisson's ratios of the three layers are arbitrarily assumed to be 0.25.

calculations for the trilayered disk are performed by arbitrarily assuming Poisson's ratio of 0.25 for all three layers while other material properties and dimensions remain unchanged, and the corresponding results are shown in Fig. 5(a) and (b), respectively, for the stresses at the tensile surface and the biaxial stress in the central region through the thickness. Excellent agreement between analytical and FEA results is obtained. Based on the results shown in Figs. 4 and 5, the following issue is raised. When the layers have very different Poisson's ratios, is there a way to improve the accuracy of the closed-form solutions for the stress distributions given by Eq. (22)? This issue is addressed as follows.

For the strength measurement, the biaxial stresses in the central region bounded by the inner ring are of concern. Under the biaxial-stress condition, $\varepsilon_r = \varepsilon_\theta$ and Eqs. (3a) and (3b) become

$$\sigma_{ri} = \sigma_{\theta i} = E_i^*(1 + v_i)\varepsilon_r \quad (i = 1\text{–}n). \tag{23}$$

However, it should be noted that the approximation of $v_i = v$ is used in the parentheses in Eqs. (3a) and (3b) in deriving the closed-form solution for the position of the neutral surface; i.e., Eq. (5), for multilayers. This approximation corresponds to

$$\sigma_{ri} = \sigma_{\theta i} = E_i^*(1 + v)\varepsilon_r \quad (i = 1\text{–}n). \tag{24}$$

While Eq. (23) is exact, Eq. (24) is approximate which leads to the solution described by Eq. (22). However, if Eq. (24) is multiplied by a factor of $(1 + v_i)/(1 + v)$, it becomes identical to Eq. (23). Hence, the accuracy of the closed-form solutions for the stress distributions given by Eq. (22) can be improved by multiplying a factor of $(1 + v_i)/(1 + v)$. For example, this factor corresponds to 0.967, 0.905, and 1.021, respectively, for LSM, NiO-YSZ, and YSZ which compensates the errors of the analytical solutions shown in Fig. 4(b).

5. Concluding remarks

Biaxial flexure tests have been used extensively to measure the biaxial strength of brittle materials. However, the tests and analyses are limited to materials of uniform properties. An analytical model is developed in the present study to analyze stress distributions in thin multilayered disks subjected to biaxial flexure tests. It is found that closed-form solutions for multilayered disks can be obtained from existing solutions for monolayered disks by replacing the position of the neutral surface and the flexural rigidity of the specimen. To validate the present analytical solutions for multilayers, the finite element analysis is performed on an LSM/YSZ/NiO-YSZ trilayered disk subjected to ring-on-ring tests, and good agreement between analytical and numerical results is obtained. The present closed-form solutions hence provide a basis for evaluating the biaxial strength of multilayered systems. Depending upon the strength of the individual layer and the stress distribution through the thickness of the multilayer during testing, cracking can initiate from any layer under tension. However, it should be noted that because the difference in Poisson's ratio between layers is ignored in determining the position of the neutral surface analytically, the stresses in layers with Poisson's ratios greater than the average Poisson's ratio are slightly under-predicted and the stresses in layers with Poisson's ratios smaller than the average Poisson's ratio are slightly over-predicted (see Fig. 4(b)). To compensate the errors in predicted stresses caused by different Poisson's rations between layers, stresses given by Eq. (22) should be multiplied by a factor of $(1 + v_i)/(1 + v)$ where v_i is the Poisson's ratio of the individual layer and v is the average Poisson's ratio of the multilayer. The physical meaning of this multiplication factor is given in Section 4.

Finally, it is worth mentioning that multilayered disks are generally subjected to residual thermal stresses because of the thermomechanical mismatch between layers, and the disks can be curved. While flat specimens are required in testing, slight out-of-flatness can be compensated by using compliant rings or placing a sheet of rubber or silicon between the supporting ring and specimen (ASTM Standard, 2003). To minimize friction, an appropriate lubricant or placing a sheet of carbon foil or Teflon tape between the loading ring and the specimen is recommended. Also, closed-form solutions for thermal stresses in multilayers have been derived previously (Townsend et al., 1987; Hsueh, 2002), and resultant stresses in the specimen can be obtained by superposing the thermal stresses on the stresses due to biaxial flexure tests.

Acknowledgments

The authors thank Dr. M. Radovic for useful comments. This research was jointly sponsored by the Laboratory Directed Research and Development Program of Oak Ridge National Laboratory (CHH), and US Department of Energy, Division of Materials Sciences and Engineering, Office of Basic Energy under contract DE-AC05-00OR22725 with UT-Battelle, LLC.

References

Arai, A., Kobayashi, O., Takagi, F., Akioka, K., Shimoda, T., 1994. Mechanical properties of hot-rolled Pr–Fe–B–Cu magnets. Journal of Applied Physics 75 (10), 6631–6633.

ASTM C 1499-03, 2003. Standard Test Method for Monotonic Equibiaxial Flexural Strength of Advanced Ceramics at Ambient Temperature. ASTM International, West Conshohocken, Pennsylvania.

Bassali, W.A., 1957. The transverse flexure of thin elastic plates supported at several points. Proceedings Cambridge Philosophical Society 53, 728–743.

Brett, R.L., Rowlinson, N., Ashraf, M.M., Harris, I.R., Bowen, P., 1990. Magnetic and mechanical properties of rotary forged aluminum compacted Nd–Fe–B magnets. Journal of Applied Physics 67 (9), 4622–4624.

Hehn, L.P., Chen, Z., Mecholsky, J.J., Klocek, P., Hoggins, J.T., Trombetta, J.M., 1994. Fracture surface analysis of free-standing diamond films. Journal of Materials Research 9 (6), 1540–1545.

Hsueh, C.H., 2002. Modeling of elastic deformation of multilayers due to residual stresses and external bending. Journal of Applied Physics 91 (12), 9652–9656.

Li, J.F., Pan, W., Sato, F., Watanabe, R., 2001. Mechanical properties of polycrystalline Ti_3SiC_2 at ambient and elevated temperatures. Acta Materialia 49, 937–945.

Lucas, G.E., 1990. Review of small specimen test techniques for irradiation testing. Metallurgical Transactions 21A, 1105–1119.

Meyers, D.E., Chen, F.C., Zhang, J., Ardell, A.J., 1993. Optimization of test parameters for quantitative stress measurements using the miniaturized disk-bend test. American Society for Testing and Materials 21, 263–271.

Muskhelishvili, N.I., 1949. Some Basic Problems of the Mathematical Theory of Elasticity, 3rd ed. Moscow.

Nadai, A., 1922. Die verbiegungen in einzelnen punkten understützten kriesförmiger platten. Physik Z 23, 366–376.
Kirstein, A.F., Woolley, R.M., 1967. Symmetrical bending of thin circular elastic plates on equally spaced point supports. Journal of Research of the National Bureau of Standards 71C (1), 1–10.
Ritter, J.E., Jakus, K., Batakis, A., Bandyopadhyay, N., 1980. Appraisal of biaxial strength testing. Journal of Non-Crystalline Solids 38/39, 419–424.
Selcuk, A., Merere, G., Atkinson, A., 2001. The influence of electrodes on the strength of planar zirconia solid oxide fuel cells. Journal of Materials Science 36, 1173–1182.
Shetty, D.K., Rosenfield, A.R., McGuire, P., Bansal, G.K., Duckworth, W.H., 1980. Biaxial flexure tests for ceramics. American Ceramic Society Bulletin 59 (12), 1193–1197.
Shi, J.L., Zhu, G.Q., Gao, J.H., Li, L., Lu, Z.L., Lai, T.R., 1998. Biaxial stretching of superplastic Y-TZP, Y-TZP/Al_2O_3, and Y-TZP/LAS glass composites in air atmosphere. Journal of Materials Research 13 (8), 2224–2230.
Simpatico, A., Cannon, W.R., Matthewson, M.J., 1999. Comparison of hydraulic-burst and ball-on-ring tests for measuring biaxial strength. Journal of the American Ceramic Society 82 (10), 2737–2744.
Skorvánek, I., Gerling, R., 1992. The influence of neutron irradiation on the soft magnet and mechanical properties of amorphous and nanocrystalline $Fe_{73.5}Cu_1Nb_3Si_{13.5}B_9$ alloys. Journal of Applied Physics 72 (8), 3417–3422.
Timoshenko, S., Woinowsky-Krieger, S., 1959. Theory of Plates and Shells. McGraw-Hill Book Company, New York.
Townsend, P.H., Barnett, D.M., Brunner, T.A., 1987. Elastic relationships in layered composite media with approximation for the case of thin films on a thick substrate. Journal of Applied Physics 62 (11), 4438–4444.
Vitman, F.F., Pukh, V.P., 1963. A method for determining the strength of sheet glass. Zavodskaya Laboratoriya 29 (7), 863–867.
Zeng, K., Odén, A., Rowcliffe, D., 1998. Evaluation of mechanical properties of dental ceramic core materials in combination with porcelains. The International Journal of Prosthodontics 11 (2), 183–189.